JOURNAL OF GEOPHYSICAL RESEARCH, VOL. 108, NO. D17, 4556, doi:10.1029/2002JD002979, 2003

Global teleconnections of climate to terrestrial carbon flux

C. Potter,[1] S. Klooster,[2] M. Steinbach,[3] P. Tan,[3] V. Kumar,[3] S. Shekhar,[3] R. Nemani,[4] and R. Myneni[5]

Received 24 September 2002; revised 13 May 2003; accepted 11 June 2003; published 12 September 2003.

[1] We have applied association analysis to 17 years of climate index observations and predicted net ecosystem production on land to infer short-term (monthly to yearly) teleconnections between atmosphere-ocean climate forcing and terrestrial carbon cycles. The analysis suggests that on a global level, climate indices can be significantly correlated to net ecosystem carbon fluxes over more than 58% of the nondesert/ice-covered land surface, commonly with a lead period of 2–6 months. The Southern Oscillation (SO) and Arctic Oscillation (AO) indices explain nearly equal portions of these significantly correlated area carbon fluxes. These significant teleconnections detected between surface climate and seasonal carbon gain or loss in terrestrial vegetation offer important capabilities for making inferences about the variability in the terrestrial carbon cycle of natural and agricultural ecosystems worldwide. *INDEX TERMS:* 0315 Atmospheric Composition and Structure: Biosphere/atmosphere interactions; 0322 Atmospheric Composition and Structure: Constituent sources and sinks; 1615 Global Change: Biogeochemical processes (4805); 1620 Global Change: Climate dynamics (3309); 1640 Global Change: Remote sensing; *KEYWORDS:* carbon flux, global model, ENSO

Citation: Potter, C., S. Klooster, M. Steinbach, P. Tan, V. Kumar, S. Shekhar, R. Nemani, and R. Myneni, Global teleconnections of climate to terrestrial carbon flux, *J. Geophys. Res.*, *108*(D17), 4556, doi:10.1029/2002JD002979, 2003.

1. Introduction

[2] Net photosynthetic accumulation of carbon by plants, also known as net primary production (NPP), provides the energy that drives most biotic processes on Earth. NPP produces organic matter that is consumed by microbes and animals. Sustained NPP can contribute to unique biological properties of Earth's terrestrial surface, such as the diversity of organisms supported by any given ecoclimatic zone. Moreover, climate controls on NPP fluxes are an issue of central relevance to human society, mainly because of concerns about the extent to which NPP in managed ecosystems can provide adequate food and fiber for a growing population. Predictability in the NPP fluxes of agricultural zones is a principal foundation for sustainable development. In addition, accounting for the potential of long-term entrapment of atmospheric CO_2 derived from fossil fuel pollution sources back in terrestrial ecosystems begins with an understanding of interannual to decadal climate controls on NPP and net ecosystem production (NEP) fluxes, which can further account for terrestrial carbon sinks [*Schimel et al.*, 2001].

[3] As a major biological flux of carbon, predicted NPP for a large land area is a unique integrator of climatic, ecological, geochemical and human influences on the global carbon cycle. In the absence of major human disturbance, surface temperature, precipitation, and solar irradiance have been shown as the strongest controllers of yearly terrestrial NPP at the global scale [*Lieth*, 1975; *Mellilo et al.*, 1993; *Potter et al.*, 1993]. Reliable estimates of seasonal NPP and NEP fluxes depend on timely and accurate forecasts of these climate forcing variables over land.

[4] The influence of ocean surface patterns, such as those associated with the El Niño-Southern Oscillation (ENSO), have been noted as significant global teleconnections for atmospheric circulation and land surface climate [*Glantz et al.*, 1991]. Teleconnection is a term used in meteorological studies to describe simultaneous variation in climate and related processes over widely separated points on earth. There are different phases in climate patterns such as the ENSO, which is called El Niño in the warm phase and La Niña in the cold phase. ENSO warming at the sea surface, which is driven by changes in winds and ocean-atmosphere heat exchange, typically extends to about 30°N and 30°S latitude, with lags into continental land areas of several months. Certain elements of climate variability at relatively high latitudes may be predictable from forcings by sea surface temperature (SST) and sea level pressure (SLP) in the tropical ocean [*Ting et al.*, 1996; *Hoerling et al.*, 2001]. For example, in the extratropics of the Northern Hemisphere, the deep Aleutian low that accompanies El Niño can advect warm moist air along the west coast of North America bringing warm spells to western Canada and Alaska [*Trenberth and Hurrell*, 1994]. On the timescale of several decades, increases in the frequency of the warm

[1]NASA Ames Research Center, Moffett Field, California, USA.
[2]Earth Systems Science and Policy Institute, California State University Monterey Bay, Seaside, California, USA.
[3]Department of Computer Science and Engineering, University of Minnesota, Minneapolis, Minnesota, USA.
[4]School of Forestry, University of Montana, Missoula, Montana, USA.
[5]Department of Geography, Boston University, Boston, Massachusetts, USA.

0148-0227/03/2002JD002979$09.00

phase of ENSO can account for 0.06°C of global warming from 1950–1998 [*Trenberth et al.*, 2002].

[5] Previous studies have identified global connections of interannual SST to land surface processes [*Keeling et al.*, 1995; *Myneni et al.*, 1998; *Dai et al.*, 1998; *Los et al.*, 2001]. These analyses have mainly focused on a single climate index, although *Los et al.* [2001] reported that effects of ENSO on land climate are sometimes magnified and at other times almost completely negated by the North Atlantic Oscillation (NAO). At a strictly regional scale, ENSO events have been linked to weather anomalies and crop production in the continental United States [*Carlson et al.*, 1996; *Nemani et al.*, 2001], and streamflow patterns in the Pacific northwest [*Hamlet and Lettenmeier*, 1999]. Several previous studies have documented the influence ENSO events on model predictions of NPP and annual carbon balance of Amazon forest ecosystems [*Prentice and Lloyd*,1998; *Tian et al.*, 1998; *Potter et al.*, 2001a, 2001b; *Foley et al.*, 2002]. However, large-scale teleconnections between multiple climate indices and global carbon fluxes have yet to be demonstrated, and may escape ready detection without the aid of spatial-temporal analysis tools designed specifically to uncover such associations, both weak and strong, between time series of SST/SLP anomalies and spatially explicit estimates of carbon fluxes on the land.

[6] We report here on approaches to identify and quantify global teleconnections of climate indices and terrestrial carbon flux represented by monthly NPP and NEP predicted by an ecosystem model over the period 1982–1998. The sparse coverages of observed NEP and NPP in space and time dictate using a predictive model for this analysis. The principal science question we address is "Can multiple climate index observations be used as reliable predictors of carbon flux patterns (NEP interannual variability and extreme events) over large areas of the global land surface?" To interpret these results, it is also necessary to incorporate information on when and where anomalies in NPP and NEP controllers (land surface temperature and precipitation) are linked to similar patterns in the climate indices.

2. Global Data and Models

[7] Several climate indices are of prime interest in this study of ocean-atmosphere-land teleconnections [*Trenberth and Hurrell*, 1994]. We focus here primarily on the Southern Oscillation Index (SOI) and the Arctic Oscillation (AO) index, and secondarily on two NINO indices. Correlations between these climate index anomalies and monthly gridded SST [*Bottomley et al.*, 1990; *Reynolds et al.*, 2002] for period of 1982–1998 indicate the central areas of the ocean temperature record that can be most closely associated with each the indices (Figure 1). SOI is an indicator of atmospheric impacts of ENSO, computed as the standardized difference between SLP measured in Tahiti (17°S, 149°W) and Darwin, Australia (13°S, 131°E). The AO is derived from 1000 mb height anomalies poleward of 20°N [*Thompson and Wallace*, 1998]. The NINO1 + 2 index is used to monitor SST over the eastern tropical Pacific, delineated by the area between 0°–10°S and 90°W–80°W. The NINO4 index is used to monitor SST over the area between 5°N–5°S and 160°E–150°W.

[8] The SOI and NINO indices are commonly used to document warm-phases in ENSO, which are often associated with above-average temperatures in the northwestern half of the North American continent, and below-average temperatures in the southeastern half [*Trenberth and Hurrell*, 1994; *Klein et al.*, 1999; *McCabe and Dettinger*, 1999]. There is also a pattern of the warm-phase ENSO associated with above-average precipitation over western coastal South America [*Vuille et al.*, 2000], the southern United States, and northern Mexico, plus below-average precipitation in south-central Africa, northeastern South America, parts of southern Asia and Australia, and in North America from the Canadian Rockies to the Great Lakes region.

[9] The AO is closely related to the North Atlantic Oscillation (NAO, measured between the Icelandic low (65°N, 22°W) and the Azores high pressure centers from 39°N, 9°W to 36°N, 6°W [*Walker and Bliss*, 1932]), which, in its "high index" warm phase can represent the persistence of above-average temperatures over North America and Europe, and below-average temperatures variations over North Africa and the Middle East. During winters when the AO index is high, anomalously low precipitation commonly occurs over the Canadian Arctic, central and southern Europe, the Mediterranean and Middle East. In contrast, anomalously high precipitation occurs from Iceland though Scandinavia [*Hurrell*, 1995].

[10] For this analysis with climate index teleconnections, terrestrial NPP and NEP fluxes have been computed monthly (over the period 1982–1998) at a spatial resolution of 0.5° latitude/longitude using the NASA-CASA (Carnegie-Ames-Stanford) Biosphere model [*Potter*, 1999; *Potter et al.*, 1999]. NASA-CASA is a numerical model of monthly fluxes of water, carbon, and nitrogen in terrestrial ecosystems. Our estimates of terrestrial NPP fluxes depend on inputs of global satellite observations for land surface properties and on gridded model drivers from interpolated weather station records [*New et al.*, 2000] distributed across all the continental masses. Consequently, the NASA-CASA predictions of terrestrial NPP carbon fluxes are derived with no dependence whatsoever on climate index data, nor on atmospheric circulation model predictions of surface climate patterns.

[11] Our fundamental approach to estimating terrestrial NPP is to define optimal metabolic rates for carbon fixation processes, and to adjust these rate values using factors related to limiting effects of time-varying inputs of solar radiation, air temperature (TEMP), precipitation (PREC) [*New et al.*, 2000], all from ground-based weather station data sources, plus predicted soil moisture, and land cover [*DeFries and Townshend*, 1994]. Carbon (CO_2) fixed by vegetation as NPP is estimated in the ecosystem model according to the time-varying (monthly mean) fraction of photosynthetically active radiation (FPAR) intercepted by plant canopies and a light utilization efficiency term (*e*max). FPAR is the only time-varying satellite sensor data used to drive the model.

[12] The FPAR-*e*max product is modified by gridded stress factors computed in the model for temperature (*Ta*) and moisture (*W*) to vary from month-to-month. The *e*max term is set uniformly at 0.39 g C (MJ^{-1} PAR) [*Potter et al.*, 1993], a value that has been verified globally by comparing predicted annual NPP to more than 1900 field estimates of

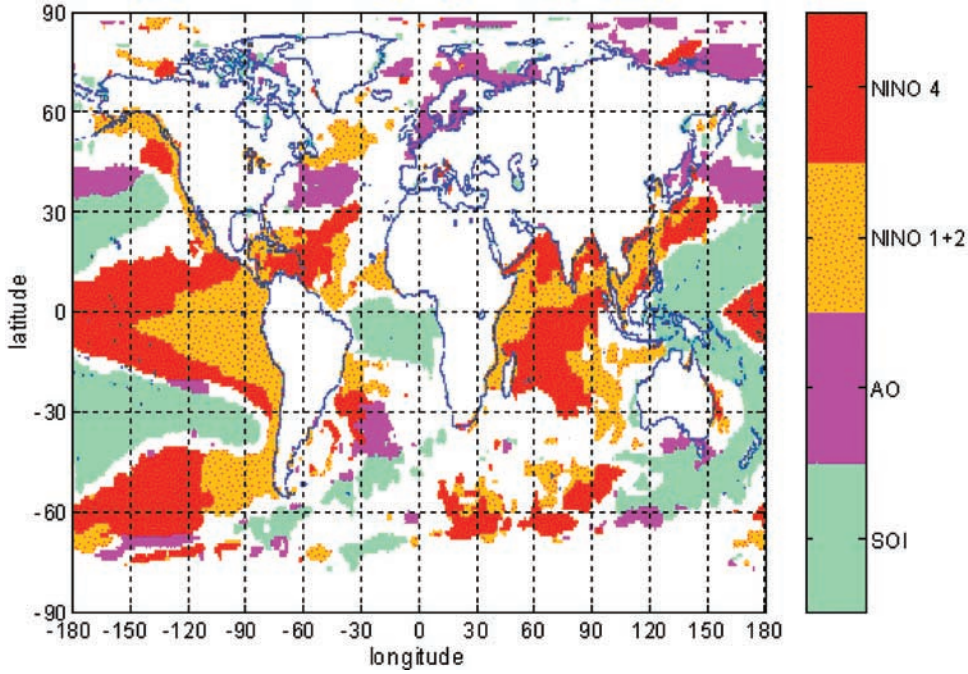

Figure 1. Areas of SST represented by correlation values of $r > 0.4$ (Pearson's coefficient) in association with the SOI, AO, NINO1 + 2, and NINO4 indices for the period 1982–1998. All time series monthly anomalies have been Z score transformed prior to cross correlation. Each nonwhite pixel indicates a pixel location where the SST record shows a significant correlation with at least one of the climate indices, and the color of that pixel indicates which of the indices has the highest correlation. Over 65% of global nonice sea coverage is represented by the four-color coverage.

NPP (Figure 2). Interannual NPP fluxes from the CASA model have been reported [*Behrenfeld et al.*, 2001] and checked for accuracy by comparison to multiyear estimates of NPP from field stations and tree rings [*Malmström et al.*, 1997]. Our NASA-CASA model has been validated against field-based measurements of NEP fluxes and carbon pool sizes at multiple boreal forest sites in North America [*Potter et al.*, 2001c; *Amthor et al.*, 2001] and against atmospheric inverse model estimates of global NEP [*Potter et al.*, 2003].

[13] Our NASA-CASA model is designed to couple seasonal patterns of NPP to soil heterotropic respiration (R_h) of CO_2 from soils worldwide [*Potter*, 1999]. First-order decay equations simulate exchanges of decomposing plant residue (metabolic and structural fractions) at the soil surface. The model also simulates surface soil organic matter (SOM) fractions that presumably vary in age and chemical composition. Turnover of active (microbial biomass and labile substrates), slow (chemically protected), and passive (physically protected) fractions of the SOM are represented. NEP can be computed as NPP minus total R_h fluxes, excluding the effects of small-scale fires and other localized disturbances or vegetation regrowth patterns on carbon fluxes [*Schimel et al.*, 2001].

[14] Whereas previous versions of the NASA-CASA model [*Potter et al.*, 1993, 1999] used a normalized difference vegetation index (NDVI) to estimate FPAR, the current model version instead relies upon canopy radiative transfer algorithms [*Knyazikhin et al.*, 1998], which are designed to generate improved spatially varying FPAR products as inputs to carbon flux calculations. These radiative transfer algorithms, developed for the MODIS (Moderate resolution Imaging Spectroradiometer) aboard the NASA Terra platform, account for attenuation of direct and diffuse incident radiation by solving a three-dimensional formulation of the radiative transfer process in vegetation canopies. Monthly gridded composite data from spatially varying channels 1 and 2 of the Advanced Very High Resolution Radiometer (AVHRR) have been processed according to the MODIS radiative transfer algorithms and aggregated over the global land surface to 0.5° grid resolution, consistent with the NASA-CASA model driver data for climate variables. The MODIS FPAR algorithms largely account for satellite orbit drift and sensor intercalibration corrections [*Myneni et al.*, 1998, 2002]. To minimize cloud contamination effects, a maximum value composite algorithm was applied spatially for 0.5° pixel values [*Knyazikhin et al.*, 1999; *Myneni et al.*, 1998]. There is no complete atmospheric correction method for water vapor and aerosols although the AVHRR 0.5° data set uses the maximum value for the compositing period which tends to minimize atmospheric contamination. Cloud screening has been performed but contamination remains in certain areas of the humid tropics and the high latitudes, and offsets have been provided in lieu of a full intercalibration between satellites.

3. Land Climate Controls on Ecosystem Carbon Fluxes

[15] Global terrestrial NPP was estimated by our NASA-CASA model to vary between 45 and 51 Pg C per year [*Potter et al.*, 1999, 2003]. The global predicted NEP flux for atmospheric CO_2 has varied between an annual source

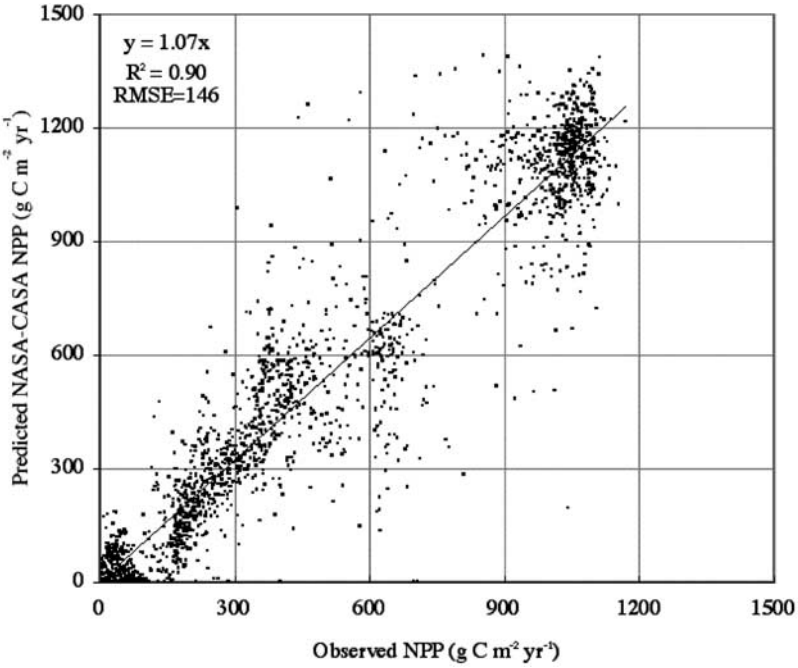

Figure 2. Comparison of annual observed NPP to predicted values from the NASA-CASA model (driven by 0.5° FPAR from the satellite AVHRR and climate means from *New et al.* [2000]). The data set of more than 1900 observed NPP points was compiled for the Ecosystem Model-Data Intercomparison (EMDI) activity by the Global Primary Productivity Data Initiative (GPPDI) working groups of the International Geosphere Biosphere Program Data and Information System (IGBP-DIS). Analysis of residuals has determined that scatter around the least squares regression line may be due as much to uncertainties in scaling and inconsistencies in the ground-based measurements of NPP reported in tropical and subtropical ecosystems as to the prediction uncertainties represented in the NASA-CASA model.

of −0.9 Pg C per year to a sink of +2.1 Pg C per year, with a trend of increasing from negative (net source flux to the atmosphere) in the early 1980s to a consistently positive (net sink flux from the atmosphere) by the mid to late 1990s. These results for NPP fluxes are all consistent with those reported by *Schimel et al.* [2001] based largely on predictions from numerous other global ecosystem models and inventories. While absolute NEP values are subject to considerable uncertainty, the anomalies, which are the basis of this study, may be realistic. Our NASA-CASA model results are also consistent with the findings of *McGuire et al.* [2001] and *Vukicevic et al.* [2001] that globally, there can be a net release of carbon to the atmosphere during El Niño years, and a net uptake during cooler non El Niño years. However, our results suggest that this climate control pattern applies mainly to the tropical zones of the terrestrial biosphere.

[16] Association rule analysis can offer further insights into the types of dependencies that exist among variables within a large data set [*Goodman and Kruskal*, 1954]. Nonrandom associations between two or more model variables are reported here using the chi-square test [*Stockburger*, 1998]. Chi-square values greater than 3.84 (degrees of freedom = 1) indicate a high probability ($p < 0.05$) of nonrandom association between anomalously low (LO) or anomalously high (HI) monthly events for TEMP or PREC with either NPP or NEP. We used an anomalous event threshold value of 1.5 standard deviations or greater from the long-term (1982–1998) monthly mean value. For our analysis, association patterns are reported below on the basis of frequency of occurrence within major global vegetation types [*DeFries and Townshend*, 1994].

[17] The main result from this analysis is that below-average PREC and above-average TEMP can, respectively, decrease predicted NPP and NEP in the tropics while increasing NPP in notable areas of tundra and boreal forests. Specifically, we find that one of the strongest nonrandom associations in our NASA-CASA results is that PREC-LO events cooccur with NPP-LO and with NEP-LO events in certain areas of evergreen broadleaf forests, deciduous broadleaf forests, croplands, and grassland savannas (Figure 3a). These events occur mainly in drought-sensitive areas of tropical and subtropical zones, and possibly in areas of major wild fires that are associated with FPAR-LO events. We also find that TEMP-HI events cooccur with NPP-LO events for these same vegetation types, which can be another indicator of drought stress effects on plant carbon gains.

[18] Another nonrandom association rule indicates that TEMP-HI events cooccur with NPP-HI and NEP-HI events in subareas of tundra, grasslands, deciduous needleleaf forests, evergreen needleleaf forests, and mixed (needleleaf-broadleaf) forest biomes (Figure 3b), even with cooccurring PREC-LO events. These observations lead to the hypothesis that regional climate warming has had the greatest impact on high latitude (tundra and

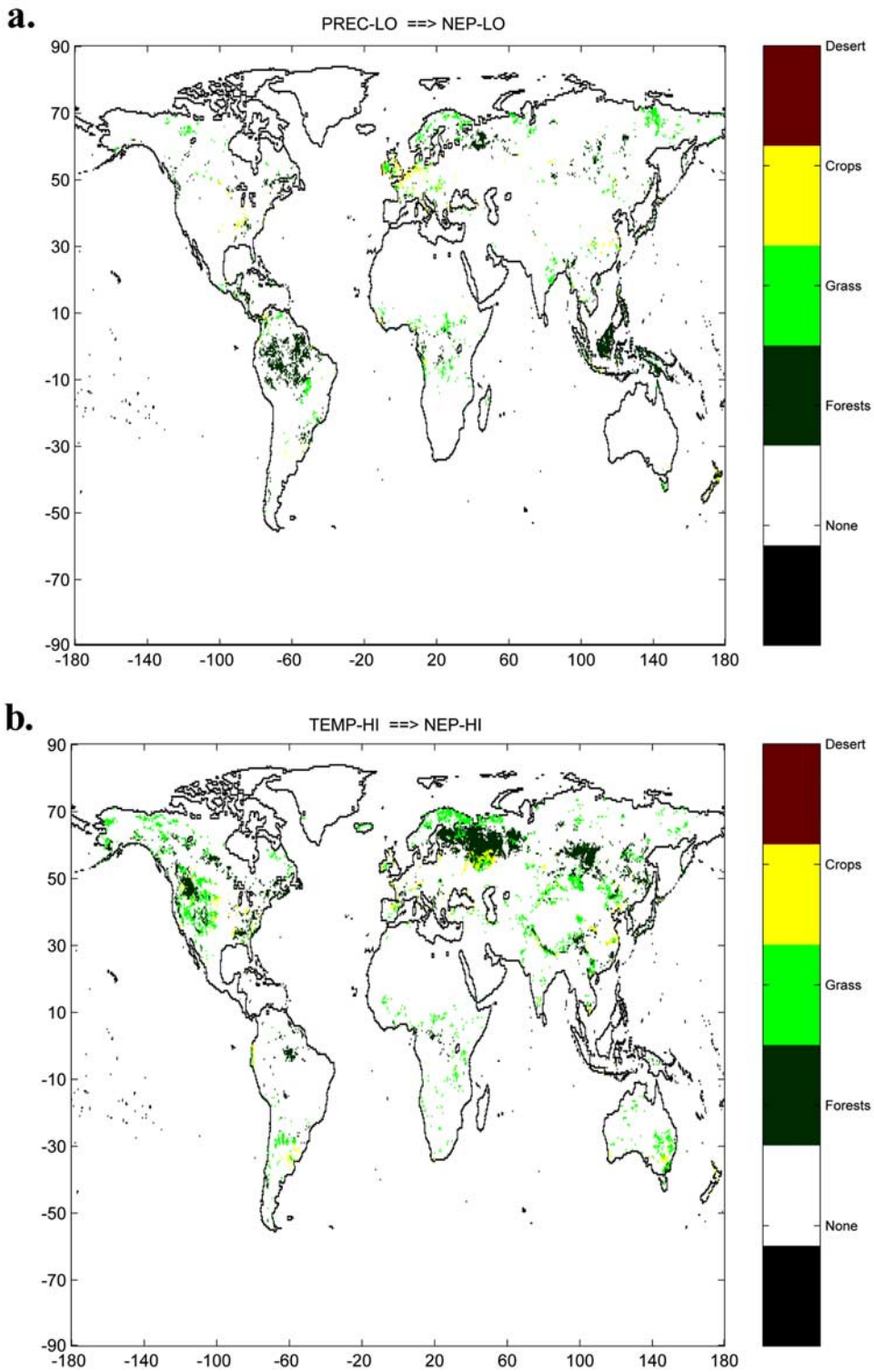

Figure 3. Locations of cooccurrence between anomalously low (LO) or anomalously high (HI) monthly event observations for climate inputs and NASA-CASA predicted NEP from 1982 to 1998. An anomalous event threshold value was defined as 1.5 standard deviations or greater from the long-term (1982–1998) monthly mean value. Each nonwhite pixel indicates a location where NEP anomalies cooccurs in the time series with (a) PREC-LO or (b) TEMP-HI, and the color of that pixel indicates the vegetation type at that location.

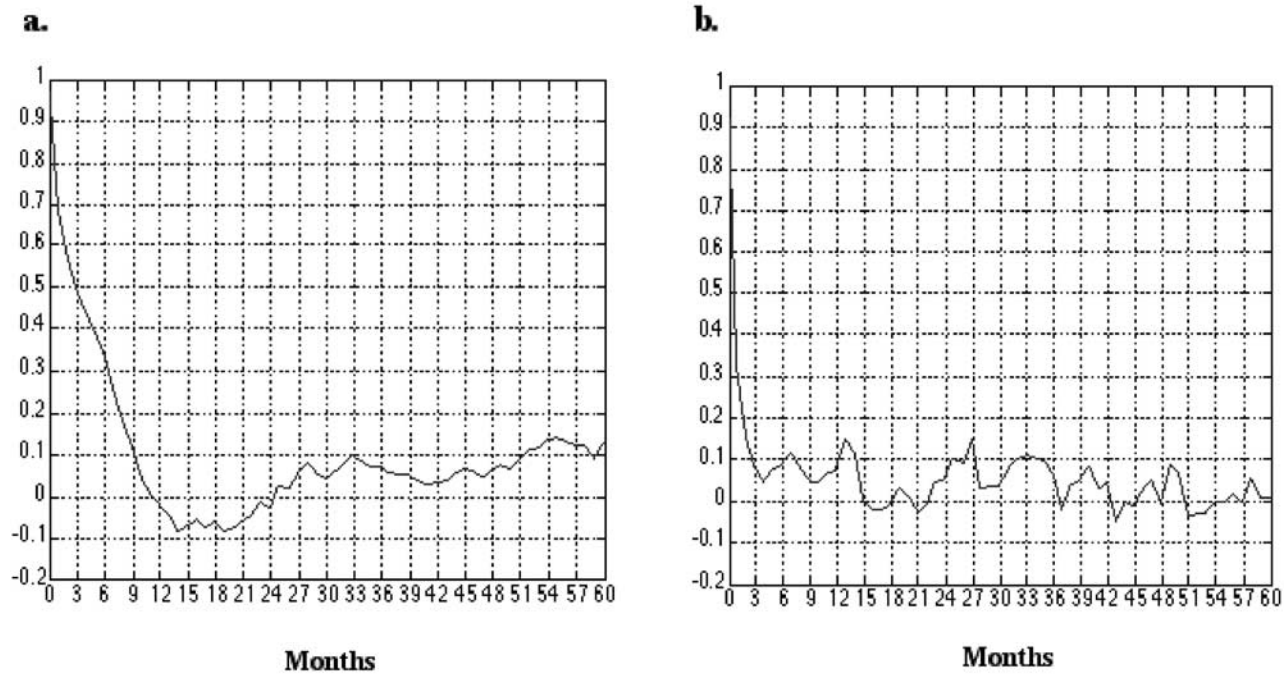

Figure 4. Autocorrelation function of (a) SOI and (b) AO indices (1958–1995) at monthly lag periods.

boreal) sinks for atmospheric CO_2, particularly over the Eurasian continent.

[19] We find in addition that PREC-HI plus TEMP-HI events cooccur with NPP-HI and NEP-HI events in subareas of mixed forests, deciduous broadleaf forests, and evergreen needleleaf forest biomes. This nonrandom association suggests an important dual control over net carbon fluxes by PREC and TEMP events in transition zones between cool temperate and warmer subtropical forest ecosystems.

4. Time Series Teleconnections

4.1. Climate

[20] As a first step in analysis of global teleconnections, we examined the underlying empirical relationships between land climate records, those used as input to the NASA-CASA model, and the four selected climate indices. We address the questions of where and how the land surface temperature and precipitation time series used as model input variables are correlated with the ENSO and AO patterns. Our analysis here covers a long-term (1958–1998) historical record to assess the impacts of ENSO and AO on land climate, rather than concentrating on individual ENSO events of the past 20 years. By considering several decades of climate cycles, we can more accurately assess the impacts of events such as El Niño and La Niña on the terrestrial biosphere, and their statistical significance.

[21] Serial correlation (i.e., autocorrelation) needs to be considered when testing significance of the association between two time series. Geophysical time series are frequently autocorrelated because of inertia or carryover processes in the physical system. The effect of autocorrelation on cross-correlations can be dealt with in various ways [*Pyper and Peterman*, 1998]. First, the number of degrees of freedom (df) can be reduced. This has the effect of increasing the cut-off value at which a correlation is considered statistically significant. A second way is to attempt to remove the autocorrelation, thereby reducing the cross-correlation in the event of autocorrelation [*Katz*, 1988]. This second method may be preferable in cases where the value of the correlation is prime interest, and secondarily whether the correlation is significant at some level. However, methods to remove autocorrelation (e.g., prewhitening) can also remove the low-frequency correlation that constitutes the main topic of interest in this study. Therefore we have chosen the first way of reducing df to a level that treats these cross-correlations as if the data showed insignificant autocorrelation starting at six month time intervals rather than at monthly intervals.

[22] Autocorrelation function (ACF) analysis is the correlation of each measurement in a times series with a measurement before or after it in the series. Autocorrelation can be assessed in the form of Pearson's product moment correlation coefficient [*Tong*, 1990]. Pearson correlation test with these climate index data sets indicates that ACF must >0.3 to be statistically different from zero (two-tailed t test [*Stockburger*, 1998]), and thereby indicate a significant autocorrelation. We determined the ACF for climate indices at all possible lag times. SOI anomalies have a low ACF (<0.3) at lag times greater than about six months (Figure 4a; using index data from 1958–1995). The same is true for the NINO1 + 2 index anomalies. For the AO/NAO anomalies, the ACF is <0.1 at lag times greater than three months Figure 4b. Like SOI patterns in Figure 4a, the ACF is <0.3 at lag times greater than six months for our predicted NPP anomalies. On the basis of these results, it is a conservative determination [*Trenberth and Caron*, 2000] to accept df for the climate index time series correlations with terrestrial carbon fluxes to be df = 32 (34 "seasons" of six months duration in a 17-year window, minus 2 for a two-tailed test

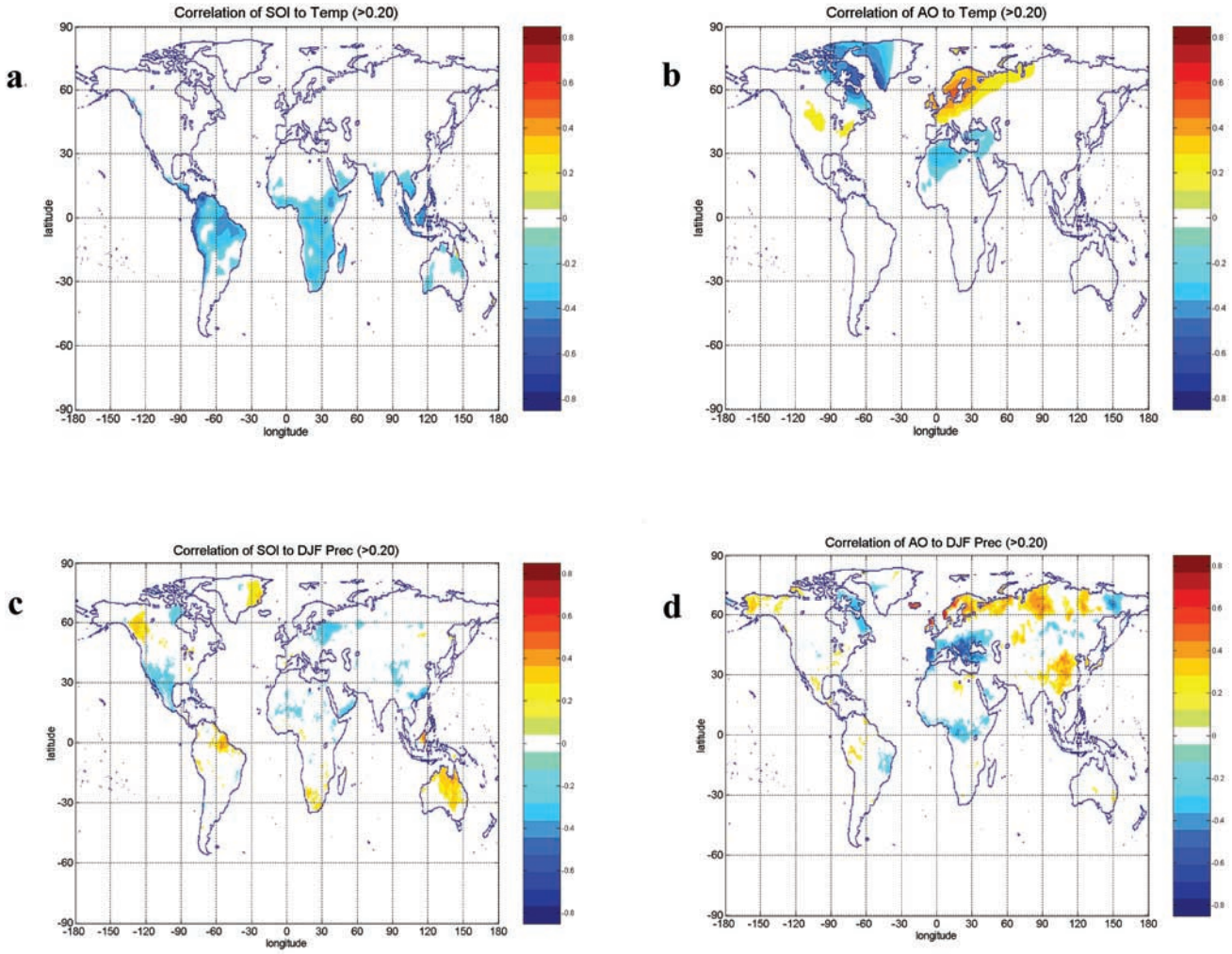

Figure 5. Global correlations ($r > 0.2$) of SOI and AO index (1958–1998) Z score anomalies with CRU05 monthly (a, b) TEMP and (c, d) PREC for the three-month period December–February (DJF).

of significance). For the purposes of demonstrating a significant association with measured climate index values at df = 32 (17-years), Pearson's correlation coefficient (r) > 0.34 carries a relatively high confidence level of $p < 0.05$. When dealing with long-term climate correlations and df > 75 (for roughly 40-years of global records), values of $r > 0.2$ carry the same confidence level of $p < 0.05$.

[23] Like *Mason and Goddard* [2001], we report on analysis of the long-term climate data from the Climate Research Unit of the University of East Anglia, Norwich [*New et al.*, 2000] (hereinafter referred to as the CRU05 data set). CRU05 is a global, monthly mean data set of TEMP, PREC, humidity, and cloudiness at 0.5° by 0.5° latitude/longitude resolution, available for the period 1901–1995. Because the land climate record is most reliable after the 1940s, we restricted our analysis to the period between 1958 and 1998.

[24] Significant correlations between the time series anomalies of the SOI, AO, NINO1 + 2 and NINO4 climate indices and 0.5° PREC or TEMP on land were identified. The first step in this analysis was the conversion of all time series to monthly Z score values, which can be used to specify the relative statistical location of each monthly value within the 40-year population distribution (e.g., all Januarys have adjusted with respect to the long-term mean January value). The numerical Z score indicates the distance from the long-term monthly mean as the number of standard deviations above or below the mean. The main difference between the t-statistic and the Z score is that the t test uses a sample standard deviation, whereas the Z score uses population standard deviation.

[25] Results show that CRU05 land TEMP records for the period 1958–98 were most significantly correlated with SOI in the tropical zones between 15°N and 30°S (Figure 5a), whereas the most significant correlation areas of TEMP with AO were located in Scandinavia, northwestern Europe, eastern and southern boarders of the Mediterranean Sea, and portions of northeastern Canada (Figure 5b). CRU05 land TEMP records were most significantly correlated with NINO1 + 2 in many of the same areas as AO (results not shown). CRU05 land TEMP records were most significantly correlated with NINO4 in Pacific coastal zones of North America and in many of the same areas of the tropical zone as SOI.

[26] Three-month seasonal subsets of the climate indices were correlated to the corresponding three-month seasonal

Table 1. Exclusive Area Coverage for Correlation Results Between Climate Indices (1958–1998) With CRU05 Monthly TEMP, PREC For 3-Month Periods, and NASA-CASA Predicted NEP (1982–1998)[a]

		PREC				
	TEMP	DJF	MAM	JJA	SON	NEP
SOI	1.7	12.9	4.1	2.8	11.6	13.2
AO	10.7	21.8	3.7	4.1	10.5	14.1
NINO1 + 2	18.1	1.3	3.5	1.4	8.9	14.5
NINO4	6.5	14.9	7.7	8.9	9.5	15.7
TOTAL	36.9	50.8	19.0	17.3	40.4	57.6

[a]Area coverage is percent of the global land surface, excluding ice and desert cover.

subsets PREC. On a global basis, land PREC correlations with all four climate indices were generally most significant during the northern hemisphere winter (DJF) and autumn (SON) months, compared to the spring (MAM) and summer (JJA) months [*Trenberth and Hurrell*, 1994; *Hurrell*, 1995]. Results show that CRU05 land DJF PREC records for the period 1958–98 were most significantly correlated with SOI in the Pacific coastal zones of central Canada, Mexico and the southwestern United States, the northeastern Amazon, eastern Europe, and Australia (Figure 5c). The most significant DJF PREC correlations with AO were located in Scandinavia, northern Eurasia, northern boarders of the Mediterranean Sea, and portions of Canada, Alaska, central South America, and Africa (Figure 5d). CRU05 land PREC records were most significantly correlated with NINO1 + 2 and NINO4 indices in areas of the southern United States and in many of the same tropical zones as SOI.

[27] We computed the "exclusive" area for the climate index correlations as follows. For each pixel where a significant correlation is found with the CRU05 variables, we select the index with the maximum correlation value and sum to the fraction of the total land area covered by this climate index. Exclusive area coverage results (Table 1) for climate index correlations with 40-year CRU05 records exclude ice and desert cover [*DeFries and Townshend*, 1994]. Highest global area coverage for combined climate index correlations (at $r > 0.2$) was with DJF PREC (51%), followed by SON PREC (40%), and land TEMP (37%). We note that AO correlations contributed higher exclusive area coverages than did SOI for global correlations with either DJF PREC or land TEMP records.

[28] On a global basis, land FPAR correlations with the four climate indices were generally most significant in areas that correspond closely to those shown with high correlations in Figures 4c and 4b for DJF PREC. These areas for significant FPAR correlations cover large sections of western and central North America, Brazil, eastern Europe, Siberia, southern Africa, and Australia.

4.2. Carbon Fluxes

[29] Turning to predicted carbon flux results, we used matching monthly records for the period of 1982–1998 to investigate associations between the time series anomalies of the climate indices and predicted carbon fluxes on land from the NASA-CASA model. Examples of the close association between three climate indices and land NPP fluxes at $r > 0.4$ are shown in Figure 6. These locations were selected because of their close proximity to land areas where climate index-NPP correlations of $r > 0.5$ are aggregated. Both the SOI and NPP fluxes (for example, in eastern Brazil) show low points in 1983, 1987, 1992, and 1998. The NINO1 + 2 index and NPP fluxes (for example, in the southwestern United States) both show high points during these same years, suggesting a reverse effect (compared to SOI) of precipitation patterns between the two distant land areas. The AO index and NPP fluxes (for example, in southern Scandinavia) both show rapid increases in 1986, 1989 and 1995, which can be attributed to increasing precipitation and temperature on land during these transition periods. We find that a seasonal phase shift in climate index lead times of up to six months commonly improved correlations with the NPP and NEP time series anomalies.

[30] Global correlation maps (Figures 7a–7c) show the areas where $r > 0.34$ for associations of the SOI, NINO1 + 2, and AO indices with our predicted NEP fluxes for the period 1982–98. Seasonality in all time series records was removed before this analysis by computing a 12-month moving average [*Bousquet et al.*, 2000]. Phase shifts (in months) are shown (Figures 7d–7f) for the most significant climate index association shown in the correlation maps. The 2–6 month lead between the climate indices and NEP results principally from phase differences between the climate indices and the model inputs (TEMP, PREC, and FPAR) used to generate NEP. We note that NEP is correlated with climate indexes based largely on TEMP, PREC and FPAR controls over NPP rather than on prediction of heterotrophic soil respiration.

[31] We find that for nearly 58% of the global nonbarren (desert/ice coverage) of the land, anomalies in deseasonalized NEP fluxes have significant teleconnections with climate (Table 1), as represented by four indices (SOI, AO, NINO1 + 2, and NINO4) associations combined. The desert and ice-covered areas excluded from our analysis were defined according to the global land cover from *DeFries and Townshend* [1994]. Each of the four climate indices used to map significant correlations with NEP contributed about 14% to the overall nonbarren coverage. For deseasonalized NPP anomalies, 56% of the nonbarren land surface has a significant teleconnection with the four climate indices. In comparison to these NASA-CASA model outputs, the FPAR input time series of deseasonalized anomalies have significant teleconnections with the four climate indices for 55% of the nonbarren land surface. Because we cannot rule out completely that FPAR values in areas like the humid tropics and the northern boreal forest may be depressed by persistent cloud or smoke aerosol contamination, these area totals for significant correlations with climate indices could be conservative estimates.

[32] Because of the high level of temporal and spatial autocorrelation in the 17-yr predicted NPP and NEP global results, it is possible that spurious (random) correlations with the four climate indices might be detected. Following the general methods described by *Wilks* [1995], we generated 1000 random time series, performed global pixel correlations with NPP and NEP, then computed the combined land area with significant correlation for sets of four random time series. We find that these sets of four random time series will correlate as significantly in terms of global

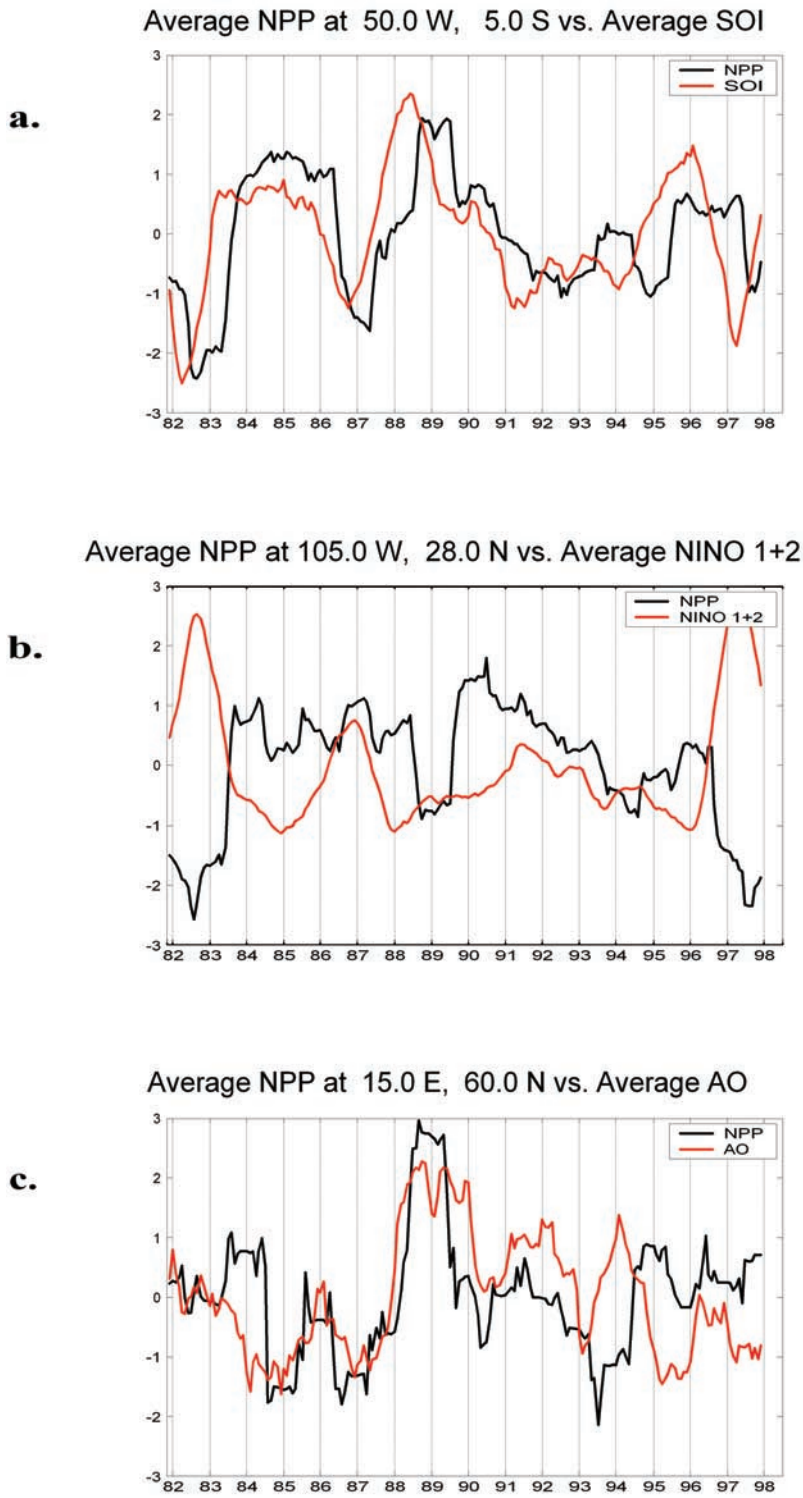

Figure 6. Time series association of 12-month running average SOI, NINO1 + 2, and AO anomalies with terrestrial NPP anomalies at $r > 0.4$ for selected areas of the (a) eastern Brazil, (b) southwestern United States, and (c) southern Scandinavia. Time series were standardized to scale between −3 and +3 by subtracting the mean of the entire time series and dividing by the overall standard deviation.

NPP coverage (56%) almost as often as do the four selected climate index time series. We next find, however, that the combined global land coverage for NEP correlations with the four selected climate indices (58%), as shown in Figure 7, is significantly higher ($p < 0.05$) than any set of four random number time series we can generate. Therefore it is highly unlikely that the four selected climate index time series correlations with global NEP is spurious.

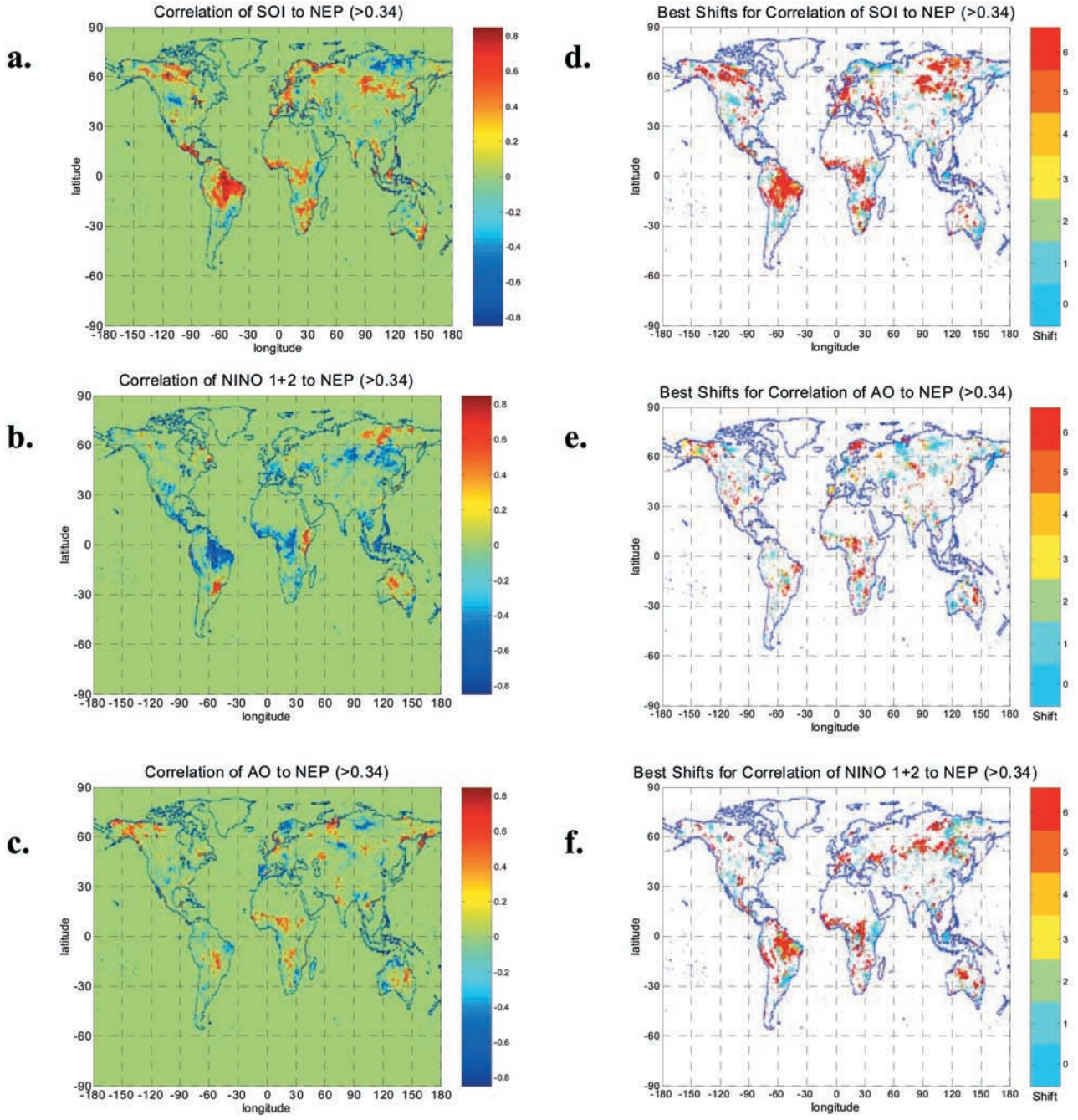

Figure 7. Global associations of SOI, NINO1 + 2, and AO anomalies with predicted terrestrial NEP anomalies (1982–1998). (a–c) Correlation coefficients are shown by the color bar for pixels correlated at $r > 0.34$, based on the lags indicated in Figures 7d–7f; (d–f) Phase shifts (in months) for the most significant associations shown in Figures 7a–7c. Twelve-month running mean anomalies were computed to deseasonalize the time series comparisons.

[33] The influences of climatic teleconnections can be observed in predicted annual carbon fluxes over some of the most drought-stressed land areas of the globe. In particular, the SOI and NINO1 + 2 indices are consistent indicators of interannual NEP fluxes in large sections of central North and South America, western and central Africa, south Asia and Australia. Teleconnections of AO are most strongly predicted with annual NEP fluxes for large sections of western Canada, Scandinavia, central Eurasia, the Mediterranean, southern Africa, and central Brazil. We note, however, that NEP in certain interior land areas of the Northern Hemisphere above 50°N latitude cannot be significantly correlated with any of the four selected climate indices.

[34] The tropical inland areas of central and southern Brazil that show significant correlations for FPAR, NPP, and NEP with AO (Figures 7c) are noteworthy, particularly because these patterns in the 17-year satellite record of terrestrial FPAR can corroborate the findings of atmospheric

simulation studies that have recently implied a strong influence of southern Atlantic SST anomalies on the NAO, with concurrent impacts on southern Amazon rainfall patterns [*Robertson et al.*, 2000]. Our results here are an additional indicator of circulation and heating patterns associated with the South American monsoon system (SAMS), which may exert an important influence on the boreal winter subtropical jet over eastern North America, possibly through changes Amazon rainfall and regional Hadley circulations [*Nogués-Paegle et al.*, 1998].

[35] The relative impacts of PREC and TEMP time series inputs (to the NASA-CASA carbon model) on correlations between climate indices SOI and AO with our predicted NEP fluxes can be examined further by comparison of Figures 5 and 7. For example, we find that 15% of total land area shown in Figure 7a as having significant correlation of NEP with SOI also shows significant correlation of DJF PREC with SOI (Figure 5c). Just over 34% of total land area shown in Figure 7a as having significant correlation of NEP with SOI also shows significant correlation of TEMP with SOI (Figure 5a), while only 7% also shows significant correlation of both PREC and TEMP with SOI. We find that 23% of the total land area shown in Figure 7c as having significant correlation of NEP with AO also shows significant correlation of DJF PREC with AO (Figure 5d), while 30% of total land area shown in Figure 7a shows significant correlation of TEMP with AO (Figure 5b), and nearly 11% also shows significant correlation of both PREC and TEMP with AO. We can conclude therefore that at least 50% of the global land areas shown in Figure 7 as having significant correlation of predicted NEP with SOI or AO results from similarly significant correlations of either PREC and TEMP model inputs with SOI or AO. The remaining 50% of the global land area shown in Figure 7 as having significant NEP correlations must result from FPAR inputs to the NASA-CASA carbon model, which can also correlate significantly with either SOI or AO.

[36] Effects in land use boundaries are detectable in our global results. When the nonbarren surface is separated into global cultivated and uncultivated areas, the total area where anomalies in annual NPP or NEP fluxes have significant correlations ($r > 0.34$) with the four climate indices is much lower for cultivated areas at 7% exclusive global coverage than for uncultivated areas at >50% exclusive global coverage. Exclusive global coverages for CRU05 TEMP and PREC correlations ($r > 0.34$) with the four climate indices are both less than 6% of the total cultivated land area. This comparison implies that land climate and carbon fluxes in cultivated areas worldwide are not as closely linked to large-scale climate teleconnections as are carbon fluxes in uncultivated "natural" ecosystems, or that cultivation occurs mainly in regions that are not strongly teleconnected to ENSO or AO.

5. Concluding Remarks

[37] This first global analysis of climate teleconnections with terrestrial carbon fluxes from satellite observations suggests a number of important lines of study for carbon cycle science. We are able to make an initial assessment of the ecosystem areas that are most strongly influenced by climate teleconnections to ocean-atmosphere processes, thereby laying the foundation for more predictive model development at the global level. The results presented here also begin to demonstrate the magnitude of temporal and spatial variability in terrestrial exchanges of CO_2 with the atmosphere that can be attributed mainly to large-scale coupling with global climate processes. Our terrestrial ecosystem model includes predictions for the amount of NPP carbon stored in vegetation biomass and soils [*Potter*, 1999; *Potter et al.*, 2001a], which makes is possible to link localized controls on atmospheric CO_2 sinks on the land to ocean-atmosphere dynamics anywhere on the globe. With an extension of our predicted terrestrial NEP record from the NASA-CASA model to more than 20 years, additional events in SST/SLP variation can be included in an attempt to establish even stronger climate-land teleconnections in the carbon cycle. For future studies of the terrestrial carbon cycle, major anomalies in ecosystem carbon fluxes to or from the pool of CO_2 in the atmosphere might be predicted based on more detailed association and statistical analyses of these kind of teleconnections.

[38] **Acknowledgments.** This work was supported by grants from NASA programs in Intelligent Systems and Intelligent Data Understanding, and the NASA Earth Observing System (EOS) Interdisciplinary Science Program. We thank Joseph Coughlan and David Peterson of NASA Ames Research Center for helpful comments on an earlier version of the manuscript.

References

Amthor, J. S., et al., Boreal forest CO_2 exchange and evapotranspiration predicted by nine ecosystem process models: Inter-model comparisons and relations to field measurements, *J. Geophys. Res.*, *106*, 33,623–33,648, 2001.

Behrenfeld, M. J., et al., Biospheric primary production during an ENSO transition, *Science*, *291*, 2594–2597, 2001.

Bottomley, M., C. K. Folland, J. Hsiung, R. E. Newell, and D. E. Parker, Global ocean surface temperature atlas "GOSTA", 20 pp., Dep. of Earth, Atmos. and Planet. Sci., Mass. Inst. of Technol., Cambridge, 1990.

Bousquet, P., P. Peylin, P. Ciais, C. Le Quéré, P. Friedlingstein, and P. P. Tans, Regional changes in carbon dioxide fluxes of land and oceans since 1980, *Science*, *290*, 1342–1346, 2000.

Carlson, R. E., D. P. Todey, and S. E. Taylor, Midwestern corn yield and weather in relation to extremes of the Southern Oscillation, *J. Prod. Agric.*, *9*, 347–352, 1996.

Dai, A., K. E. Trenberth, and T. R. Karl, Global variations in droughts and wet spells: 1900–1995, *Geophys. Res. Lett.*, *25*, 3367–3370, 1998.

DeFries, R., and J. Townshend, NDVI-derived land cover classification at global scales, *Int. J. Remote Sens.*, *15*, 3567–3586, 1994.

Foley, J. A., A. Botta, M. T. Coe, and M. H. Costa, El Niño–Southern oscillation and the climate, ecosystems and rivers of Amazonia, *Global Biogeochem. Cycles*, *16*(4), 1132, doi:10.1029/2002GB001872, 2002.

Glantz, M. H., R. W. Katz, and N. Nicholls (Eds.), *Teleconnections Linking World-wide Climate Anomalies*, 527 pp., Cambridge Univ. Press, New York, 1991.

Goodman, L. A., and W. H. Kruskal, Measures of association for cross-classifications, *J. Am. Stat. Assoc.*, *49*, 732–764, 1954.

Hamlet, A. F., and D. P. Lettenmeier, Columbia River streamflow forecasting based on ENSO and PDO climate signals, *Am. Soc. Civ. Eng.*, *25*, 333–341, 1999.

Hoerling, M. P., J. W. Hurrell, and T. Xu, Tropical origins for recent North Atlantic climate change, *Science*, *292*, 90–92, 2001.

Hurrell, J. W., Decadal trends in the North Atlantic Oscillation regional temperatures and precipitation, *Science*, *269*, 676–679, 1995.

Katz, R. W., Use of cross correlations in the search for teleconnections, *J. Climatol.*, *8*, 241–253, 1988.

Keeling, C. D., T. P. Whorf, M. Whalen, and J. van der Plicht, Interannual extremes in the rise of atmospheric carbon dioxide since 1980, *Nature*, *375*, 666–670, 1995.

Klein, S. A., B. J. Soden, and N.-C. Lau, Remote sea surface temperature variations during ENSO: Evidence for a tropical atmospheric bridge, *J. Clim.*, *12*, 917–932, 1999.

Knyazikhin, Y., J. V. Martonchik, R. B. Myneni, D. J. Diner, and S. W. Running, Synergistic algorithm for estimating vegetation canopy leaf

area index and fraction of absorbed photosynthetically active radiation from MODIS and MISR data, *J. Geophys. Res.*, *103*, 32,257–32,276, 1998.

Knyazikhin, Y., et al., MODIS leaf area index (LAI) and fraction of photosynthetically active radiation absorbed by vegetation (FPAR) product (MOD15) algorithm, theoretical basis document, NASA Goddard Space Flight Cent., Greenbelt, Md., 1999.

Lieth, H., Modeling the primary productivity of the world, in *Primary Productivity of the Biosphere*, edited by H. Lieth and R. H. Whittaker, pp. 237–263, Springer-Verlag, New York, 1975.

Los, S. O., G. J. Collatz, L. Bounoua, P. J. Sellers, and C. J. Tucker, Global interannual variations in sea surface temperature and land surface vegetation, air temperature, and precipitation, *J. Clim.*, *14*, 1535–1549, 2001.

Malmström, C. M., M. V. Thompson, G. P. Juday, S. O. Los, J. T. Randerson, and C. B. Field, Interannual variation in global scale net primary production: Testing model estimates, *Global Biogeochem. Cycles*, *11*, 367–392, 1997.

Mason, S. J., and L. Goddard, Probabilistic precipitation anomalies associated with ENSO, *Bull. Am. Meteorol. Soc.*, *82*, 619–638, 2001.

McCabe, G. J., and M. D. Dettinger, Decadal variations in the strength of ENSO teleconnections with precipitation in the western United States, *Int. J. Climatol.*, *19*, 1399–1410, 1999.

McGuire, A. D., et al., Carbon balance of the terrestrial biosphere in the twentieth century: Analyses of CO_2, climate and land-use effects with four process-based ecosystem models, *Global Biogeochem. Cycles*, *15*, 183–206, 2001.

Melillo, J. M., A. D. McGuire, D. W. Kicklighter, B. Moore III, C. J. Vorosmarty, and A. L. Schloss, Global climate change and terrestrial net primary production, *Nature*, *363*, 234–240, 1993.

Myneni, R. B., C. J. Tucker, G. Asrar, and C. D. Keeling, Interannual variations in satellite-sensed vegetation index data from 1981 to 1991, *J. Geophys. Res.*, *103*, 6145–6160, 1998.

Myneni, R., et al., Global products of vegetation leaf area and fraction absorbed PAR from year one of MODIS data, *Remote Sens. Environ.*, *83*, 214–231, 2002.

Nemani, R. R., M. A. White, D. R. Cayan, G. V. Jones, S. W. Running, and J. C. Coughlan, Asymmetric climatic warming improves California vintages, *Clim. Res.*, *19*, 25–34, 2001.

New, M., M. Hulme, and P. Jones, Representing twentieth century space-time climate variability. II. Development of 1901–1996 monthly grids of terrestrial surface climate, *J. Clim.*, *13*, 2217–2238, 2000.

Nogués-Paegle, K., C. Mo, and J. Paegle, Predictability of the NCEP-NCAR reanalysis model during austral summer, *Mon. Weather Rev.*, *126*, 3135–3152, 1998.

Potter, C. S., Terrestrial biomass and the effects of deforestation on the global carbon cycle, *BioScience*, *49*, 769–778, 1999.

Potter, C. S., J. T. Randerson, C. B. Field, P. A. Matson, P. M. Vitousek, H. A. Mooney, and S. A. Klooster, Terrestrial ecosystem production: A process model based on global satellite and surface data, *Global Biogeochem. Cycles*, *7*, 811–841, 1993.

Potter, C. S., S. A. Klooster, and V. Brooks, Interannual variability in terrestrial net primary production: Exploration of trends and controls on regional to global scales, *Ecosystems*, *2*, 36–48, 1999.

Potter, C. S., V. Brooks-Genovese, S. A. Klooster, M. Bobo, and A. Torregrosa, Biomass burning losses of carbon estimated from ecosystem modeling and satellite data analysis for the Brazilian Amazon region, *Atmos. Environ.*, *35*, 1773–1781, 2001a.

Potter, C. S., S. Klooster, C. R. de Carvalho, V. Brooks-Genovese, A. Torregrosa, J. Dungan, M. Bobo, and J. Coughlan, Modeling seasonal and interannual variability in ecosystem carbon cycling for the Brazilian Amazon region, *J. Geophys. Res.*, *106*, 10,423–10,446, 2001b.

Potter, C. S., J. Bubier, P. Crill, and P. LaFleur, Ecosystem modeling of methane and carbon dioxide fluxes for boreal forest sites, *Can. J. For. Res.*, *31*, 208–223, 2001c.

Potter, C. S., S. A. Klooster, R. B. Myneni, V. Genovese, P.-N. Tan, and V. Kumar, Continental scale comparisons of terrestrial carbon sinks estimated from satellite data and ecosystem modeling 1982–1998, *Global Planet. Change*, in press, 2003.

Prentice, I. C., and J. Lloyd, C-quest in the Amazon basin, *Nature*, *396*, 619–620, 1998.

Pyper, B. J., and R. M. Peterman, Comparison of methods to account for autocorrelation in correlation analyses of fish data, *Can. J. Fish. Aquat. Sci.*, *55*, 2127–2140, 1998.

Reynolds, R. W., N. A. Rayner, T. M. Smith, D. C. Stokes, and W. Wang, An improved in situ and satellite SST analysis, *J. Clim.*, *15*, 1609–1625, 2002.

Robertson, A. W., C. R. Mechoso, and Y.-J. Kim, The influence of Atlantic sea surface temperature anomalies on the North Atlantic Oscillation, *J. Clim.*, *13*, 122–138, 2000.

Schimel, D., et al., Recent patterns and mechanisms of carbon exchange by terrestrial ecosystems, *Nature*, *414*, 169–172, 2001.

Stockburger, D. W., Introductory statistics: Concepts, models, and applications, WWW version 1.0, Southwest Mo. State Univ., Springfield, 1998. (Available at http://www.psychstat.smsu.edu/sbk00.htm)

Thompson, D. W. J., and J. M. Wallace, The Arctic Oscillation signature in the wintertime geopotential height and temperature fields, *Geophys. Res. Lett.*, *25*, 1297–1300, 1998.

Tian, H. Q., J. M. Melillo, D. W. Kicklighter, A. D. McGuire, J. V. K. Helfrich, B. Moore, and C. J. Vorosmarty, Effect of interannual climate variability on carbon storage in Amazonian ecosystems, *Nature*, *396*, 664–667, 1998.

Ting, M., M. P. Hoerling, T.-Y. Xu, and A. Kumar, Northern Hemisphere teleconnection patterns during extreme phases of the zonal mean circulation, *J. Clim.*, *9*, 2614–2623, 1996.

Tong, H., *Nonlinear Time Series: A Dynamical System Approach*, Oxford Univ. Press., New York, 1990.

Trenberth, K. E., and J. M. Caron, The Southern Oscillation revisited: Sea level pressures, surface temperatures and precipitation, *J. Clim.*, *13*, 4358–4365, 2000.

Trenberth, K. E., and J. W. Hurrell, Decadal atmosphere-ocean variations in the Pacific, *Clim. Dyn.*, *9*, 303–319, 1994.

Trenberth, K. E., J. M. Caron, D. P. Stepaniak, and S. Worley, Evolution of El Niño–Southern Oscillation and global atmospheric surface temperatures, *J. Geophys. Res.*, *107*(D8), 4065, doi:10.1029/2000JD000298, 2002.

Vuille, M., R. S. Bradley, and F. Keimig, Climate variability in the Andes of Ecuador and its relation to tropical Pacific and Atlantic sea surface temperature anomalies, *J. Clim.*, *13*, 2520–2535, 2000.

Vukicevic, T., B. H. Braswell, and D. Schimel, Diagnostic study of temperature controls on global terrestrial carbon exchange, *Tellus, Ser. B*, *53*, 150–170, 2001.

Walker, G. T., and E. W. Bliss, World weather V, *Mem. R. Meteorol. Soc.*, *4*, 53–84, 1932.

Wilks, D. S., *Statistical Methods in the Atmospheric Sciences: An Introduction*, *Int. Geophys. Ser.*, vol. 59, 464 pp., Academic, San Diego, Calif., 1995.

S. Klooster, Earth Systems Science and Policy Institute, California State University Monterey Bay, 100 Campus Center, Seaside, CA 93955, USA.

V. Kumar, S. Shekhar, M. Steinbach, and P. Tan, Department of Computer Science and Engineering, University of Minnesota, Minneapolis, MN 55455, USA.

R. Myneni, Department of Geography, Boston University, 675 Commonwealth Avenue, Boston, MA 02215, USA.

R. Nemani, School of Forestry, University of Montana, Missoula, MT 59812, USA.

C. Potter, NASA Ames Research Center, Mail Stop 242-4, Moffett Field, CA 94035, USA. (potter@gaia.arc.nasa.gov)